PHYSICAL REVIEW D **85,** 115014 (2012)

Supersoft supersymmetry is super-safe

Graham D. Kribs[1] and Adam Martin[2]

[1]*Department of Physics, University of Oregon, Eugene, Oregon 97403, USA*
[2]*Theoretical Physics Department, Fermilab, Batavia, Illinois 60510, USA*

(Received 30 March 2012; published 19 June 2012)

We show that supersymmetric models with a large Dirac gluino mass can evade much of the jets plus missing energy searches at the LHC. Dirac gaugino masses arise from "supersoft" operators that lead to finite one-loop suppressed contributions to the scalar masses. A little hierarchy between the Dirac gluino mass 5–10 times heavier than the squark masses is automatic and technically natural, in stark contrast to supersymmetric models with Majorana gaugino masses. At the LHC, colored sparticle production is suppressed not only by the absence of gluino pair (or associated) production, but also because several of the largest squark pair production channels are suppressed or absent. We recast the null results from the present jets plus missing energy searches at the LHC for supersymmetry onto a supersoft supersymmetric simplified model. Assuming a massless lightest supersymmetric particle, we find the strongest bounds are as follows: 748 GeV from a $2j + \not{E}_T$ search at ATLAS (4.7 fb^{-1}) and 684 GeV from a combined jets plus missing energy search using α_T at CMS (1.1 fb^{-1}). In the absence of a future observation, we estimate the bounds on the squark masses to improve only modestly with increased luminosity. We also briefly consider the further weakening in the bounds as the lightest supersymmetric particle mass is increased.

DOI: 10.1103/PhysRevD.85.115014 PACS numbers: 12.60.Jv

I. INTRODUCTION

The parameter space of the minimal supersymmetric standard model (MSSM) is significantly constrained by impressive searches at the LHC. The strongest limits occur on the mass of colored superpartners, well over 1 TeV in simplified models in which the squark or gluino decays to a quark or gluon and a (nearly) massless lightest supersymmetric particle (LSP). These limits are driven by several search strategies for large missing energy and large amounts of hadronic activity, which we abbreviate $nj + \not{E}_T$.

The strong constraints from $nj + \not{E}_T$ searches have (re)motivated three basic approaches to weak-scale supersymmetry:

(1) Discard superpartners that are not directly relevant to electroweak symmetry breaking, including the first and second generation squarks. Well-known examples are more minimal supersymmetry [1,2] and split supersymmetry [3]. The extent to which these approaches successfully retain a light third generation with heavy first and second generations has been explored recently in several scenarios [4–11].

(2) Keep superpartners roughly in the sub-TeV region, while removing most or all of the *missing energy*, thereby rendering $nj + \not{E}_T$ searches moot. The classic example is R-parity violation (for a review, see [12]) through the baryon number violating $u^c d^c d^c$ term in the superpotential, which allows the LSP to decay into jets (for a recent discussion see [13–16]).

(3) Keep superpartners roughly in the sub-TeV region, while removing most or all of the *visible energy*, which significantly weakens the effectiveness of $nj + \not{E}_T$ searches. This approach includes compressed supersymmetry [17], stealth supersymmetry [18] (which is a hybrid between approaches 2 and 3), and others.

In this paper, we propose a fourth alternative:

(4) Keep most superpartners in the sub-TeV region, while removing much of the *production cross section*, thereby significantly weakening the effectiveness of $nj + \not{E}_T$ searches. We demonstrate that this alternative allows first and second generation squarks to be as light as ~650–750 GeV with a massless LSP, and potentially even lighter if there is modest compression by either raising the LSP mass or allowing a cascade decay through intermediate mass superpartners. The key to this alternative is to assume the gluino acquires a large Dirac mass.

Reducing the production cross section of colored superpartners "merely" by raising the Majorana gluino mass in the MSSM would seem to be just as sufficient. However, the squark masses receive substantial log-enhanced contributions to their masses through renormalization group evolution. This includes the stop masses, which in turn feed into the Higgs soft masses through the top Yukawa. Since the Higgs soft masses directly determine the fine-tuning of the electroweak symmetry breaking scale, this implies the stops as well as the gluino should not far exceed the electroweak scale without causing excessive unnaturalness.

A heavy Dirac gluino, by contrast, is completely natural [19–22]. Dirac gaugino masses induce one-loop finite contributions to squark, slepton, and Higgs soft masses from "supersoft" operators [22]. The finiteness implies that

renormalization group evolution of squark masses is insensitive to the gaugino masses, preserving the little hierarchy $M_3 \simeq (5\text{–}10) \times M_{\tilde{q}}$. The only price we pay is minimality—the matter content must be extended by three gauge adjoint superfields, one for each gauge group.

II. SIMPLIFIED MODELS AND THE SSSM

We are interested in calculating the bounds on supersymmetric models with Dirac gaugino masses. Our approach is to first construct a supersoft supersymmetric simplified model (SSSM) on which we can apply the $nj + \not{E}_T$ limits from the LHC. This is completely analogous to the construction of simplified models of the MSSM [23,24], which are now widely used in presenting the results from LHC searches for supersymmetry. The SSSM, illustrated in the far left panel of Fig. 1, has a gluino with a large, purely Dirac mass, degenerate first and second generation squarks (of both handedness), and the lightest supersymmetric particle (LSP) at the bottom of the spectrum. In defining the SSSM, we have explicitly chosen the Dirac gluino mass to have a fixed large value, $M_3 = 5$ TeV. The large gluino mass implies that gluino pair production is kinematically forbidden, while associated gluino/squark production is highly suppressed, leaving squark production as the only potentially viable colored sparticle production at the LHC. Squarks decay through $\tilde{q} \to q + \text{LSP}$, where the quark flavor and chirality depend on the initial squark.

To perform an apples-for-apples comparison of the constraints on supersoft supersymmetry versus the MSSM, we calculate the bounds not only on the SSSM, but also on three other simplified models of the MSSM. In all of the simplified models, the first and second generation squarks are degenerate and the LSP is massless. The spectra of the three comparison simplified models of the MSSM are shown in the three right-most panels of Fig. 1. The purpose of the comparison models is to both validate our analysis against the actual bounds from experimental analyses (where available) and to directly show the weakness of the bounds on the SSSM in direct contrast to the MSSM. The "equal MSSM" and "intermediate MSSM" simplified models are chosen to provide a comparison with typical MSSM spectra. The "heavy MSSM" simplified model is highly unnatural within the usual MSSM, as we have already discussed. Nevertheless, it illustrates the differences in squark mass bounds that remain between a heavy Majorana gluino versus a heavy Dirac gluino even when they have the same mass.

Our analyses generally assume the LSP has a kinematically negligible mass. In the Discussion we also consider the weakening of the bounds as the LSP mass is increased. The LSP could be a light gravitino, or it could instead be some other light neutral superpartner, so long as the squark decay proceeds directly to the LSP in the one step process $\tilde{q} \to q + \text{LSP}$. We also assume all decays into the LSP are prompt. The assumption of short decay chains from heavy squarks to a massless LSP implies the bounds we obtain are the most optimistic possible using the jets plus missing energy searches with no leptons in the final state.

Mapping the bounds from the SSSM onto theories with Dirac gaugino masses is straightforward in principle, though model dependent in practice. In particular, we do not include electroweak gauginos or Higgsinos in our spectrum. The supersoft supersymmetric model has heavy Dirac gaugino masses, with an ordinary MSSM μ-term for the

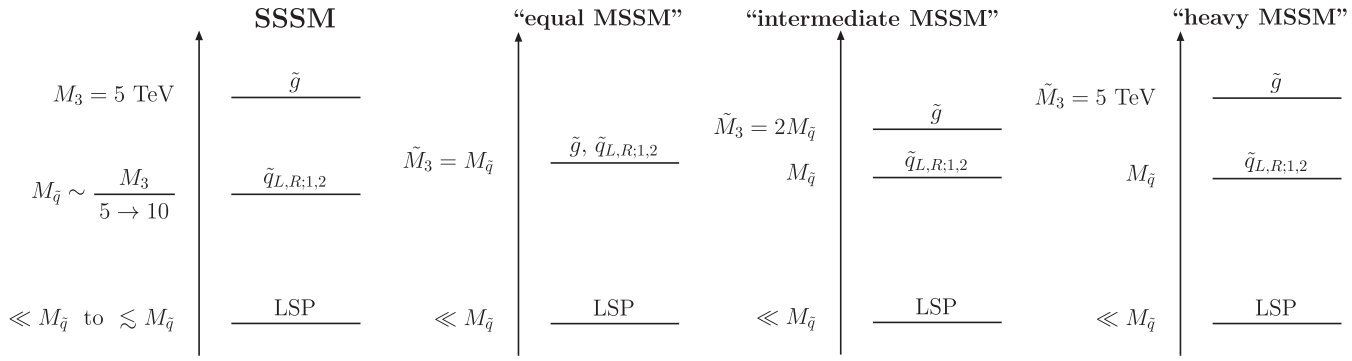

FIG. 1. The spectra for the simplified models considered in this paper. The left-most panel illustrates our primary interest—the SSSM. It contains a gluino with a large Dirac mass $M_3 = 5$ TeV, first and second generation squarks that are roughly 5–10 times lighter than gluino, and a LSP that is generally assumed to be much lighter than the squarks. The three right-most panels illustrate the three simplified models of the MSSM to which we compare. We write the gluino Dirac mass as M_3 to be distinguished from a Majorana mass written as $\tilde{M}_3$. Two of the comparison simplified models of the MSSM (equal MSSM and intermediate MSSM) are designed to provide comparisons between typical MSSM spectra and the SSSM. The third comparison model, heavy MSSM, directly compares the results for a Dirac gluino versus a Majorana gluino of the same mass. Generally, the LSP mass is taken to be kinematically negligible; however, we also comment on the relaxation of the bounds on the SSSM when the LSP is heavier.

Higgs sector [22]. Several other models incorporate Dirac gauginos [25–39]. In several cases, the gaugino sector approximately preserves a $U(1)_R$ symmetry, while the Higgs sector does not. In [31] a fully R-symmetric supersymmetric model was constructed that incorporated not only Dirac gaugino masses but also R-symmetric Higgsino masses. In this model, additional R-symmetric contributions to the soft masses were allowed and, notably, could be nearly arbitrary in flavor space. Several phenomenological implications of Dirac gauginos, as well as fully R-symmetric supersymmetry, have been explored in [40–62].

In this study we do not consider bounds on the third generation squarks. Third generation squarks receive modifications to their masses through their interactions with the Higgs supermultiplets. Given that supersoft supersymmetry has a suppressed D-term for the Higgs potential, typically this requires heavier stop masses as well as separating the scalar masses of the adjoint superfields from the corresponding Dirac gaugino masses. This could be accomplished through additional R-symmetric F-term contributions to their masses. In any case, third generation squarks have distinct signals involving heavy flavor (with or without leptons), and thus require incorporating a much larger class of LHC search strategies. We believe there are interesting differences between the third generation phenomenology of a supersoft model versus the MSSM, but we leave this for future work.

We also do not consider potentially large flavor violation in the squark-gaugino (or squark-gravitino) interactions, as could occur in an R-symmetric model [31]. This would add to the heavy flavor component of signals while subtracting from the $nj + \not{E}_T$ signals that concern us in this paper. In the interests of demonstrating the differences between the SSSM and the simplified models of the MSSM, the latter of which cannot have large flavor violation, we do not consider flavor violation in the squark interactions of the SSSM.

III. ASPECTS OF DIRAC GAUGINO MASSES

A. Supersoftness

A supersoft supersymmetric model contains chiral superfields in the adjoint representation of each gauge group of the SM in addition to the superfields of the MSSM. Supersymmetry breaking communicated through a D-term spurion leads to Dirac gaugino masses that pair up the fermionic component from each field strength with the fermionic component of the corresponding adjoint superfield. The adjoint superfields also contain a complex scalar, whose real and imaginary component masses are not uniquely determined in terms of the Dirac gaugino mass. The Lagrangian for this setup, in terms of four-component spinors, is given in Appendix A.

The scalar components of chiral superfields receive one-loop *finite* contributions to their soft masses from gauginos and adjoint scalars, as was shown clearly by [22],

$$M_{\tilde{f}}^2 = \sum_i \frac{C_i(f)\alpha_i M_i^2}{\pi} \log\frac{\tilde{m}_i^2}{M_i^2}. \quad (1)$$

The sum runs over the three SM gauge groups where $C_i(f)$ is the quadratic Casimir of the fermion f under the gauge group i. The $\tilde{m}_i$ are the soft masses for the real scalar components of the adjoint superfields. The M_i are the Dirac masses for the gauginos. Assuming the contribution to the squark masses is dominated by the Dirac gluino,

$$M_{\tilde{q}}^2 \simeq (700\ \text{GeV})^2\left(\frac{M_3}{5\ \text{TeV}}\right)^2 \frac{\log\tilde{r}_3}{\log 1.5}, \quad (2)$$

where $\tilde{r}_i \equiv \tilde{m}_i^2/M_i^2$. Somewhat smaller or larger soft masses can be achieved by adjusting the ratio $\tilde{r}_3$, since we hold the Dirac gluino mass $M_3 = 5$ TeV fixed in the SSSM.

B. Naturalness

The up-type Higgs mass squared $m_{H_u}^2$ receives positive one-loop finite contributions from the Dirac electroweak gauginos, as well as negative one-loop contributions from the stops. As was emphasized in Ref. [22], the latter contribution can easily overwhelm the former, leading to a negative Higgs mass squared and thus radiative electroweak symmetry breaking. Unlike the MSSM, however, the usual logarithmic divergence from the stop contributions to the Higgs mass is cut off by the Dirac gluino mass, giving

$$\delta m_{H_u}^2 = -\frac{3\lambda_t^2}{8\pi^2} M_{\tilde{t}}^2 \log\frac{M_3^2}{M_{\tilde{t}}^2}. \quad (3)$$

Using Eq. (1), and approximating $\log[M_3^2/M_{\tilde{t}}^2] \simeq \log[3\pi/(4\alpha_s)]$, we obtain

$$\delta m_{H_u}^2|_{\text{SSSM}} \simeq -\left(\frac{M_3}{22}\right)^2 \frac{\log\tilde{r}_3}{\log 1.5}. \quad (4)$$

Contrast this expression with the analogous one from the MSSM [7],

$$\delta m_{H_u}^2|_{\text{MSSM}} \simeq -\left(\frac{\tilde{M}_3}{4}\right)^2\left(\frac{\log\Lambda/\tilde{M}_3}{3}\right)^2, \quad (5)$$

where $\tilde{M}_3$ corresponds to the Majorana gluino mass. This makes it clear that a Dirac gluino can be several times larger than a Majorana gluino in an MSSM-type model and yet be *just as natural*, even when comparing against an MSSM model with a mediation scale that is as low as conceivable, $\Lambda \simeq 20\tilde{M}_3$. Our choice of Dirac gluino mass $M_3 = 5$ TeV with $\tilde{r}_3 \simeq 1.5$ is thus roughly equivalent, in the degree of naturalness, to a low-scale mediation MSSM model with Majorana gluino mass $\tilde{M}_3 \simeq 900$ GeV.

C. Colored sparticle production

For LHC phenomenology, there are several implications of a heavy Dirac gluino. First, gluino pair production and

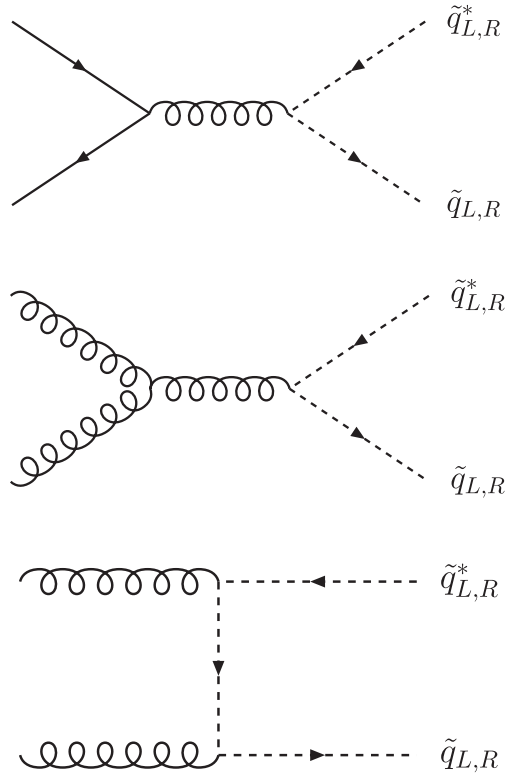

FIG. 2. The dominant tree-level Feynman diagrams for squark production at the LHC in the SSSM. Dirac gluino t-channel exchange diagrams (not shown) are suppressed by $1/M_3^2$ and thus negligible. In the MSSM, by contrast, Majorana gluino exchange is suppressed by $1/\tilde{M}_3$, and thus relevant even when $\tilde{M}_3$ is large, as shown in Fig. 3.

associated gluino/squark production is completely negligible due to the kinematic suppression. Squark-antisquark production can proceed at tree level through $gg, q\bar{q} \to \tilde{q}_L\tilde{q}_L^*, \tilde{q}_R\tilde{q}_R^*$, while the t-channel Dirac gluino exchange diagrams are suppressed by a factor $1/M_3^2$. There are also mixed-handedness production processes $pp \to \tilde{q}_L\tilde{q}_R, \tilde{q}_L^*\tilde{q}_R^*$ through t-channel gluino exchange, but again suppressed by $1/M_3^2$ in the amplitude. The contribution of these Dirac gluino exchange diagrams with $M_3 = 5$ TeV are at the level of a few percent—far smaller than the NLO QCD corrections—and thus negligible. The remaining tree-level unsuppressed Feynman diagrams that contribute to squark production are shown in Fig. 2. We emphasize that all of these subprocesses require sea quarks or gluons to initiate at the LHC.

The MSSM also contains the same-handedness processes $pp \to \tilde{q}_L\tilde{q}_L$, $\tilde{q}_R\tilde{q}_R$ through t-channel Majorana gluino exchange, leading to contributions suppressed by just one power of the gluino mass, $1/\tilde{M}_3$. These processes, as well as the mixed-handedness ones ($pp \to \tilde{q}_L\tilde{q}_R, \tilde{q}_L^*\tilde{q}_R^*$), are initiated by two valence quarks and can lead to a large fraction of the total $pp \to$ (colored superpartner) cross section. In the SSSM, the same-handedness processes are simply absent (no chirality-flipping Majorana mass), while the mixed-handedness processes are more suppressed by $1/M_3^2$ instead of $1/\tilde{M}_3$. This means the cross section for squark production in the SSSM can thus be smaller by a factor of 3 or more even when comparing the SSSM ($M_3 = 5$ TeV) against the heavy MSSM simplified model ($\tilde{M}_3 = 5$ TeV). Also, the difference between the SSSM and the MSSM grows as the squark mass increases, because the final state requires more energy, and thus higher partonic x, where valence quark distributions dominate over gluons or sea quark distributions.

D. Electroweak inos

The SSSM, by definition, does not include the effects of the Higgsinos or electroweak gauginos. For general electroweak ino masses, there are two potential effects on our results: squark cross sections could change due to virtual Higgsino or electroweak gaugino exchange; squark decay chains could change due to cascades through Higgsinos or electroweak gauginos.

Higgsino exchange contributions to first and second generation squark production is negligible, due to the small Yukawa couplings. Electroweak gaugino exchange is suppressed by the smaller electroweak couplings, and thus not relevant unless the electroweak gauginos are significantly lighter than the squarks. We thus do not expect our squark production cross section calculations to be significantly affected by the Higgsino and electroweak gaugino spectrum.

Moreover, while the masses of the electroweak gauginos are model dependent, a supersoft supersymmetric model would predict the electroweak gauginos to be $\simeq 4\pi/g$ heavier than sleptons. Imposing the LEP II bound on slepton masses implies the electroweak gauginos are generically heavier than the masses of the squarks we consider in this paper. Thus, squark cascade decay through electroweak gauginos is kinematically forbidden in supersoft models, and thus we do not need to consider it further.

Higgsinos, however, may be lighter than both the squarks and the electroweak gauginos. Naturalness—obtaining the right electroweak symmetry breaking vacuum without significant tuning—certainly favors lighter Higgsinos. Squark cascade decay through Higgsinos would lead to changes in the energies of the decay products, as well as the potential addition of charged leptons or neutrinos in the final state. Detailed simulation of these cases is highly model dependent. Nevertheless, the jets plus missing energy bounds on models with lighter Higgsinos could be substantially weaker if the average hadronic activity is reduced. On the other hand, the bounds from other supersymmetric searches could be substantially stronger if the squark cascade through Higgsinos results in hard leptons or photons. We note, however, that searches more specific to models with Majorana neutralinos, such as same-sign lepton final states, may not yield strong bounds if the model is approximately R-symmetric, and so again we are left with model-dependent investigations to make quantitative statements.

IV. RECASTING LHC LIMITS

To recast LHC limits on colored superparticle production into the SSSM, we follow the analyses searching for supersymmetry through $nj + \not{E}_T$ signals performed by ATLAS [63] and CMS [64–66]. Of the existing supersymmetry searches, jets plus missing energy is the simplest, and it involves the fewest assumptions about the spectrum.

To simulate the supersymmetric signal, we use PYTHIA6.4 [67]; the first and second generation squarks are set to have equal mass, the gravitino is chosen to be the LSP, and all other superpartners are decoupled (set to 5 TeV). We use CTEQ6L1 parton distribution functions, generating a sufficient number of events such that statistical fluctuations have negligible effect on our results. To incorporate detector effects into our signal simulations, all events are passed through the DELPHES [68] program using ATLAS or CMS detector options and adopting the corresponding experiment's jet definitions: anti-k_T, $R = 0.4$ for the ATLAS search [63], and anti-k_T, $R = 0.5$ for the CMS searches [64–66]. We repeat the same steps for the three simplified models of the MSSM (cf. Fig. 1), allowing all combinations of $\tilde{q}\,\tilde{q}$, $\tilde{q}^*\tilde{q}^*$, $\tilde{q}\tilde{q}^*$, as well as gluino pair production and associated squark plus gluino production. Note that our heavy MSSM simplified model is an existing CMS simplified model, "T2" [69].

Colored superpartner production cross sections receive sizable next-to-leading order (NLO) corrections. To incorporate these corrections, we feed the spectra into PROSPINO [70], restricting the processes appropriately for each simplified model (i.e., just $pp \to \tilde{q}\tilde{q}^*$ for the SSSM). The cross sections are shown in Fig. 3 for each of the simplified models as a function of squark mass. Depending on the scale choice and the squark mass, we find the K-factor ranges from 1.7–2.1. This factor takes into account the increased rate at NLO, though not the kinematic distribution of events.

The analyses we are interested in, [63–66], are broken up into several channels. For some analyses the channels are orthogonal, while in other analyses one event can fall into multiple channels. To set limits we begin by counting the number of supersymmetry events in each analysis channel for several squark masses. The number of supersymmetric events passing cuts is translated into a mass-dependent acceptance for each channel. We then form the 95% CL limit, using the likelihood ratio test statistic [71]:

$$0.05 = \frac{\int_0^\infty db' \sum_0^{N_{i,\mathrm{obs}}} \frac{(\mu_{i,b}+\mu_{i,s})^{N_{i,\mathrm{obs}}} e^{-(\mu_{i,b}+\mu_{i,s})}}{(N_{i,\mathrm{obs}})!} G(\mu_b, b')}{\int_0^\infty db' \sum_0^{N_{i,\mathrm{obs}}} \frac{\mu_b^{N_{i,\mathrm{obs}}} e^{-\mu_b}}{(N_{i,\mathrm{obs}})!} G(\mu_b, b')}. \quad (6)$$

Here $\mu_{i,b} \equiv N_{i,\mathrm{exp}}$ is the number of expected SM background events and $\mu_{i,s} \equiv N_{i,\mathrm{SUSY}}$ is the number of signal events. To estimate the effects of systematic errors, the number of SM events is modulated by a Gaussian weighting factor [72]. Specifically, we shift $\mu_b \to \mu_b(1 + f_b)$, where f_b is drawn from a Gaussian distribution centered at zero

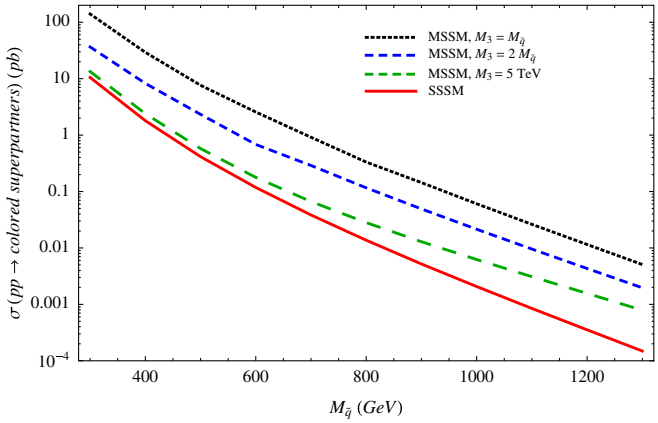

FIG. 3 (color online). Cross sections at the 7 TeV LHC for colored superpartner production. The four lines correspond to the four simplified models shown in Fig. 1, where the first and second generation squarks are degenerate with mass $M_{\tilde{q}}$. The solid line shows the cross section for the SSSM where the cross section is dominated by $\tilde{q}\tilde{q}^*$ final states, while the dashed lines show cross sections for the three simplified models of the MSSM. All cross sections are calculated to next-to-leading order using PROSPINOV2.1 [70], CTEQ6L1 parton distribution functions, and default scale choices. For event generation, we use PYTHIA6.4 [67] and rescale the cross section to match those shown here.

and with standard deviation $\sigma_f = \sigma_{i,\mathrm{SM}}/N_{i,\mathrm{exp}}$, where $\sigma_{i,\mathrm{SM}}$ is the quoted systematic uncertainty (taken directly from [63–66]). Whenever the systematic error is asymmetric, we use the larger (in absolute value) number. To combine channels (when appropriate), we simply replace the right-hand side of Eq. (6) with the product over all channels.

The number of supersymmetry events in a particular channel is the product of the cross section, luminosity, acceptance, and efficiency,

$$N_{i,\mathrm{SUSY}} = \mathcal{L} \cdot K(M_{\tilde{q}})\sigma(M_{\tilde{q}}) \cdot A(M_{\tilde{q}}) \cdot \epsilon, \quad (7)$$

where $K(M_{\tilde{q}})$ is the mass-dependent K-factor to account for the larger rate at NLO. Within our simplified setup, the only parameter the cross section and acceptance depend upon is the mass of the squark—thus Eq. (6) is simply a limit on the squark mass.

While the likelihood ratio test statistic is particularly well suited to analyses with low event counts, it is just one possibility. To test that our results do not depend on this choice, we have also computed limits using the sum-χ^2 test statistic,

$$\sum_{i=1}^{\mathrm{chan}} \frac{(N_{i,\mathrm{obs}} - (N_{i,\mathrm{exp}} + N_{i,\mathrm{SUSY}}))^2}{N_{i,\mathrm{exp}} + N_{i,\mathrm{SUSY}} + \sigma_{i,\mathrm{SM}}^2}. \quad (8)$$

We find that our results using different test statistics are broadly consistent, with the biggest differences being, as expected, when the number of events in a particular channel is low.

The constructions in Eqs. (6) and (8) are only approximate. Both formulations assume that a Gaussian treatment of the systematics is appropriate, and correlations among uncertainties when combining channels are completely neglected. A more complete treatment of the correlated experimental uncertainties may be possible through RECAST [73], which we leave for future work.

The exact limits we can place from the experimental analyses depend on several factors. The luminosity and the systematic uncertainties on the background are examples of factors that evolve with time, while the signal cross section and acceptance (for a given analysis) are fixed. To make our study as general as possible, we show our derived acceptances as a function of squark mass in a series of figures in Appendix B. These numbers allow us to estimate limits as the luminosity increases, at least for a fixed analysis strategy. Nevertheless, we do calculate the squark mass limits using the experiments' quoted luminosities and background uncertainties in Table I. Both the limits from individual channels and the combined limits (in cases where the channels are distinct and nonoverlapping) are given. The cross sections have already been shown in Fig. 3, leaving the derived acceptance times efficiency as the only undetermined factor in Eq. (7).

In the following subsections, we present the set of analyses used to bound the parameter space of our SSSM. The details of the analyses cuts can be found in Refs. [63–66]. For ease of comparison, all of the bounds we obtain for each analysis strategy from each experiment are presented in Table I. The table provides the bounds on the SSSM, as well as the three simplified models of the MSSM shown in Fig. 1. In the following, we discuss the important observables for each analysis, then describe our extracted limits.

A. ATLAS limits with 4.7 fb^{-1}

The first analysis we consider is the ATLAS jets plus missing energy search performed in Ref. [63]. Events with no leptons and large missing energy are subjected to several subanalyses, each with a different jet multiplicity requirement (2–6 jets). Within each multiplicity subanalysis, cuts are then placed on the individual jet transverse momenta, the effective mass for a given multiplicity [$m_{\mathrm{eff}}(N) = \sum_{i=1}^{N} p_{T,i} + \not{E}_T$], and the ratio of missing energy to effective mass. To further reduce backgrounds from poorly measured QCD jets, a cut is also placed on the minimum azimuthal angle between the missing momenta vector and any (sufficiently hard) jet. Surviving events are then classified according to their inclusive $m_{\mathrm{eff}}(\mathrm{inc})$, which differs from $m_{\mathrm{eff}}(N)$ in that all jets with $p_T > 40$ GeV are included in the sum. The $m_{\mathrm{eff}}(\mathrm{inc})$ classifications are referred to as "loose," "medium," and "tight." There are 11 total channels, since not every jet multiplicity has all three $m_{\mathrm{eff}}(\mathrm{inc})$ classifications.

The derived $A(M_{\tilde{q}}) \cdot \epsilon$ for the 11 different channels in the ATLAS jets plus missing energy search [63] are shown in Fig. 5 in Appendix B. We show the acceptance times efficiency as a function of squark mass both in the SSSM and in the simplified models of the MSSM.

We emphasize that Fig. 5 only gives a piece of the limit calculation—a large efficiency does not necessarily mean a good limit, as the background may also be large. Applying Eq. (8) using the observed event counts from Ref. [63], we find the 2-jet (A, A′) channels have the best sensitivity: $M_{\tilde{q}} > 737$ GeV and $M_{\tilde{q}} > 748$ GeV, respectively (95% CL, see Table I for full details). For the simplified models of the MSSM, we find the bounds range from $M_{\tilde{q}} > 1063$ GeV (for the heavy MSSM simplified model) to $M_{\tilde{q}} > 1453$ GeV (for the equal MSSM simplified model). The acceptance/efficiency factors for the different scenarios are similar, as shown in Fig. 5 in Appendix B, and thus the difference in the limits is driven by the larger cross sections in the simplified models of the MSSM.

There is a another ATLAS supersymmetry search focusing on *very* high jet multiplicity, ≥ 6 jets [74]. This search is most sensitive to supersymmetric events with long decay chains, such as from gluino pair production. For events dominated by short decay chains, i.e., the SSSM, we expect that the high-multiplicity tails are not large enough to be seen over the background uncertainty. We verified this by passing the SSSM through the analysis strategy following Ref. [74], where we find the limits are indeed poor in comparison to the other strategies, and so we do not present them.

B. CMS limits with ~1–5 fb^{-1}

We now turn to supersymmetry searches performed by the CMS Collaboration. We follow three different jets plus $\not{E}_T$ search strategies. The first, in Ref. [64], uses the α_T variable to distinguish signal—events with real missing energy—from background events where the missing energy comes from mismeasurement. The second, Ref. [65], relies on large $\not{E}_T$ and H_T to suppress background, while the third uses the so-called *razor* variables developed in [75]. We follow the same procedure as in Sec. IV A; we derive $A(M_{\tilde{q}}) \cdot \epsilon$ for each analysis using Monte Carlo events, then follow Eq. (6) to set limits on the squark masses. The $A(M_{\tilde{q}}) \cdot \epsilon$ curves depend only on the analysis cuts and can be applied unchanged to future data sets with increased luminosity or improved background modeling.

1. Search based on α_T, 1.1 fb^{-1}

In addition to basic identification cuts, this analysis requires that the leading two jets have $p_T > 100$ GeV and that the leading jet lies within the tracker. After vetoing events with leptons or photons, events are binned according to their overall $H_T = \sum_i^{\mathrm{jets}} E_{T,i}$, starting with $H_T = 275$ GeV: two 50 GeV bins spanning up to 375 GeV,

TABLE I. Channel-by-channel and combined observed limits on the simplified models illustrated in Fig. 1 using the likelihood ratio test statistic. Channels marked with asterisks have limits lower than 300 GeV, while the strongest channel for a given analysis is shown in bold. Combined limits are shown for analyses where the individual channels are orthogonal.

Search channel	SSSM ($M_3 = 5$ TeV)	Equal MSSM ($\tilde{M}_3 = M_{\tilde{q}}$)	Intermediate MSSM ($\tilde{M}_3 = 2 \times M_{\tilde{q}}$)	Heavy MSSM ($\tilde{M}_3 = 5$ TeV)
ATLAS jets + $\not{E}_T$ 4.7 fb^{-1}				
SRA (2j) medium	737 GeV	1245 GeV	1096 GeV	890 GeV
SRA (2j) tight	634 GeV	**1453 GeV**	**1305 GeV**	**1063 GeV**
SRA′ (2j) tight	**748 GeV**	1189 GeV	1061 GeV	861 GeV
SRB (3j) tight	537 GeV	1342 GeV	1202 GeV	848 GeV
SRC (4j) loose	566 GeV	973 GeV	770 GeV	584 GeV
SRC (4j) medium	634 GeV	1095 GeV	894 GeV	670 GeV
SRC (4j) tight	**	1082 GeV	831 GeV	431 GeV
SRD (5j) tight	383 GeV	1076 GeV	803 GeV	484 GeV
SRE (6j) loose	**	731 GeV	500 GeV	328 GeV
SRE (6j) medium	491 GeV	979 GeV	712 GeV	521 GeV
SRE (6j) tight	**	933 GeV	634 GeV	388 GeV
CMS α_T 1.14 fb^{-1}				
$H_T \in [275, 325)$ GeV	396 GeV	528 GeV	489 GeV	399 GeV
$H_T \in [325, 375)$ GeV	454 GeV	594 GeV	533 GeV	473 GeV
$H_T \in [375, 475)$ GeV	509 GeV	698 GeV	631 GeV	548 GeV
$H_T \in [475, 575)$ GeV	**540 GeV**	786 GeV	694 GeV	**570 GeV**
$H_T \in [575, 675)$ GeV	487 GeV	859 GeV	770 GeV	565 GeV
$H_T \in [675, 775)$ GeV	373 GeV	932 GeV	833 GeV	460 GeV
$H_T \in [775, 875)$ GeV	**	960 GeV	806 GeV	**
$H_T \geq 875$ GeV	**	**1160 GeV**	**968 GeV**	**
Combined	684 GeV	1178 GeV	1032 GeV	786 GeV
CMS jets + MHT 1.1 fb^{-1}				
$\not{E}_T > 350$ GeV, $H_T > 500$ GeV	**593 GeV**	989 GeV	844 GeV	648 GeV
$H_T > 800$ GeV	500 GeV	989 GeV	799 GeV	563 GeV
$\not{E}_T > 500$ GeV, $H_T > 800$ GeV	416 GeV	**1154 GeV**	**981 GeV**	**661 GeV**
CMS *razor*, 4.4 fb^{-1}				
0 ℓ, S1	**	639 GeV	**	**
0 ℓ, S2	**	**	**	**
0 ℓ, S3	**	960 GeV	783 GeV	434 GeV
0 ℓ, S4	**	**1082 GeV**	**898 GeV**	349 GeV
0 ℓ, S5	485 GeV	779 GeV	653 GeV	514 GeV
0 ℓ, S6	**505 GeV**	794 GeV	690 GeV	**556 GeV**
Combined	588 GeV	1137 GeV	961 GeV	677 GeV

four 100 GeV bins, then one bin containing all events with $H_T > 875$ GeV.

The hadronic activity in each event is massaged into two pseudojets[1] which are used to calculate α_T, defined as

$$\alpha_T = \frac{E_{T,2}}{M_{T,jj}}. \tag{9}$$

Cutting at $\alpha_T > 0.55$, the pure QCD contribution to the background becomes highly suppressed.

The acceptance times efficiency derived for each channel of this analysis is shown in Fig. 6 in Appendix B. The squark mass directly sets the net transverse energy in an event, so the peak efficiency in a particular H_T bin simply tracks the squark mass.

[1]For events with only two jets this massaging is trivial. For events with multiple jets, the jets are combined until the event contains only two pseudojets. The choice of how the jets are added is determined by minimizing the difference between the scalar sum of the jet E_T between the two pseudojets. See Ref. [64].

As before, the channel-by-channel limits from this search are shown in Table I. For the SSSM and the heavy MSSM simplified model, the most sensitive channels are for midrange H_T, where the signal rate is still large and the background uncertainties are falling. In comparison, the cross section for the other two simplified models of the MSSM falls much slower with increasing squark mass, propped up by the lighter Majorana gluinos, leading to the highest H_T bins being the most constraining. As the different H_T channels are orthogonal, it is straightforward to combine them, resulting in a better limit. Forming the product of likelihood ratios over all channels, we find an observed 95% CL limit of $M_{\tilde{q}} \gtrsim 684$ GeV for the SSSM and $M_{\tilde{q}} \gtrsim 786$ GeV for the heavy MSSM simplified model. The latter limit is in good agreement with the observed limit shown for the T2 simplified model in Ref. [69], giving confidence that we have successfully reproduced their analysis. For the other cases, the combined limits are much higher: $M_{\tilde{q}} \gtrsim 1160$ GeV for the equal MSSM simplified model and $M_{\tilde{q}} > 1032$ GeV for the intermediate MSSM simplified model.

2. Search based on $\not{E}_T$, H_T, 1.1 $\mathbf{fb}^{-1}$

The second CMS search strategy we consider is more traditional in that it is based simply on large multiplicity of high-p_T jets and large missing energy (see Ref. [65]). At least three jets of $p_T > 50$ GeV, $|\eta| < 2.5$ are required, and no leptons ($p_T > 10$ GeV, $|\eta| < 2.5$) are permitted. Selected events require a minimum $\not{E}_T$ or 200 GeV sufficiently separated from the jets[2] and a minimum $H_T = 350$ GeV. Passing events are piled into three further categories depending on $\not{E}_T$, H_T: (i) $\not{E}_T > 350$ GeV, $H_T > 500$ GeV, (ii) $H_T > 800$ GeV, (iii) $\not{E}_T > 500$ GeV, $H_T > 800$ GeV.

The acceptance/efficiency factors we find for the three channels are shown in Fig. 7 in Appendix B. This analysis has similar trends to the previous search. The channel with the lowest $\not{E}_T$ and H_T is the most constraining for the supersoft and heavy-gluino MSSM, while the channel with the tightest cuts is more stringent for the light gluino MSSM scenarios. The strongest individual channel limits are quite similar to the α_T case. As the channels are not orthogonal, we do not combine them; we simply quote the strongest individual channel: $M_{\tilde{q}} > 593$ GeV (SSSM), $M_{\tilde{q}} > 1154$ GeV ("light MSSM" simplified model), $M_{\tilde{q}} > 981$ GeV (intermediate MSSM simplified model), $M_{\tilde{q}} > 661$ GeV (heavy MSSM simplified model).

[2]All jets $p_T > 30$ GeV, $|\eta| < 5.0$ are used in the $\not{E}_T$ calculation, and the minimum separation is $\Delta\phi(j_i, \not{E}_T) > 0.5$ for the hardest two jets and 0.3 for the third hardest jet.

3. Search based on razor variables

The final CMS search strategy we consider from Ref. [66] utilizes the *razor* variables to discriminate signal from background. For the *razor* analysis, all objects passing basic identification and selection cuts are grouped into two "megajets." The division of particles into megajets is determined by which combination yields megajets that are closest in invariant mass. Once the megajets are formed, one boosts longitudinally to the frame where the two megajets have equal and opposite momenta along the beam direction (p_z). In this special frame, one calculates M_T^R and M_R, defined as

$$(M_T^R)^2 = \tfrac{1}{2}(\not{E}_T(p_{T,j_1} + p_{T,j_2}) - \vec{\not{E}}_T \cdot (\vec{p}_{T,j_1} + \vec{p}_{T,j_2})),$$
$$M_R = \sqrt{(E_{j_1} + E_{j_2})^2 - (p_{z,j_1} + p_{z,j_2})^2}. \tag{10}$$

The magnitude of M_R and the ratio $R^2 = (M_T^R/M_R)^2$ are then used to differentiate signal and background. The cut values for R^2 and M_R depend on whether the event contains any isolated electrons or muons. For our signal, events with isolated leptons are rare, so we focus on the hadronic channel. The events in each channel are divided up into several bins, then compared to the background, which has been extrapolated from a signal-free "fit-region."

To set limits, we considered the six analysis regions defined by Ref. [66]:

$$S_1\text{: } R^2 \in [0.18, 0.3], \quad M_R \in [2.0\text{ TeV}, 3.5\text{ TeV}];$$
$$S_2\text{: } R^2 \in [0.3, 0.5], \quad M_R \in [2.0\text{ TeV}, 3.5\text{ TeV}];$$
$$S_3\text{: } R^2 \in [0.18, 0.5], \quad M_R \in [1.0\text{ TeV}, 2.0\text{ TeV}];$$
$$S_4\text{: } R^2 \in [0.3, 0.5], \quad M_R \in [1.0\text{ TeV}, 2.0\text{ TeV}];$$
$$S_5\text{: } R^2 \in [0.2, 0.3], \quad M_R \in [650\text{ GeV}, 1.0\text{ TeV}];$$
$$S_6\text{: } R^2 \in [0.4, 0.5], \quad M_R \in [400\text{ GeV}, 1.0\text{ TeV}].$$

The acceptance times efficiency factor for each channel as a function of squark mass is shown in Fig. 8 in Appendix B.

Since the six regions are orthogonal, we can combine channels, leading to the following limits: $M_{\tilde{q}} > 588$ GeV (SSSM), $M_{\tilde{q}} > 677$ GeV (heavy MSSM simplified model), and $M_{\tilde{q}} \gtrsim 1$ TeV for the equal MSSM and intermediate MSSM simplified models with lighter Majorana gluinos. For the simplified models with heavy gluinos, the colored superpartner cross section falls fastest with increasing $M_{\tilde{q}}$, and thus the bounds are dominated by the lowest M_R bins. As the gluino mass decreases, the superpartner cross section falls less precipitously, and the larger M_R bins provide stronger constraints.

The limits we set with the six-bin approach are conservative estimates. Utilizing an unbinned likelihood approach (as done in Ref. [66]), our limits may improve. However, the unbinned approach requires a complete, smooth description of the background (and signal) in the two-dimensional (R, M_R) plane and makes our limit more sensitive to details of the detector modeling and correlations among systematics.

V. LUMINOSITY EXTRAPOLATION

It is interesting to extrapolate the squark mass limits set in the previous section out to higher luminosity. Since we do not have the observed data from the future, we extrapolate using the expected limit, meaning $N_{i,\mathrm{obs}}$ is set equal to $N_{i,\mathrm{exp}}$ in Eq. (6). As we want to vary the luminosity, the background number of events is actually $N_{i,\mathrm{ex}} \times (\mathcal{L}/\mathcal{L}_0)$, where $\mathcal{L}_0$ is the luminosity used to derive efficiencies (the luminosity in [63–66]), and $\mathcal{L}$ is the projection luminosity. This extrapolation is conservative in that it assumes there is no reoptimization of the analysis cuts and that the systematic uncertainties remain unchanged.

We perform an extrapolation using the individual channel with the strongest limits from the various analyses, as well as the combined channels for the CMS α_T strategy and the CMS *razor* strategy. These extrapolations are shown in Fig. 4. As the luminosity increases, we find the limits on the squark mass do not improve dramatically. The CMS α_T search appears to be the best-performing future search on the SSSM, with improvements on the squark mass bounds expected to be roughly 15%–25%. The limits asymptote fairly quickly once the analyses become dominated by systematic uncertainties rather than by statistical uncertainties. If the background systematics improve in the future, these projections could easily be redone using the signal acceptance times efficiency curves shown earlier.

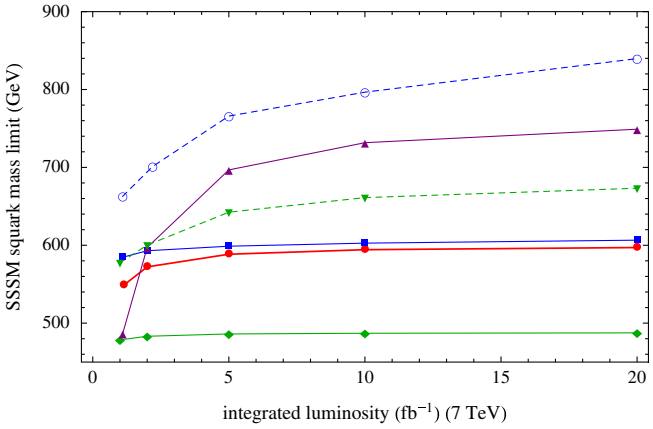

FIG. 4 (color online). Projection of the expected limits to larger integrated luminosity, holding the analysis strategy fixed as well as $\sqrt{s} = 7$ TeV. For each detector analysis strategy, the strongest individual channel is shown, while for the α_T and *razor* analyses we show the projection of the combined channel limit as well. The solid red line (with filled circles) corresponds to CMS jets plus $\not{E}_T$, the blue (with squares or open circles) corresponds to CMS α_T (solid is the single channel limit, dashed is the combined limit), green (solid and dashed with diamonds and triangles, respectively) shows CMS *razor*, and purple (with triangles) is ATLAS jets + $\not{E}_T$. We emphasize that we have plotted only the *expected* limits, to be distinguished from the *observed* limits that we show in Table I. The small differences between the expected and observed limits are at roughly the 10% level, characteristic of background fluctuations.

VI. DISCUSSION

We have shown that our simplified model of supersoft supersymmetry is clearly much less constrained by LHC searches for supersymmetry than comparable simplified models of the MSSM. We find the bounds on first and second generation squark masses in the SSSM to be between 680 to 750 GeV, depending on the experiment, the particular search strategy, and the amount of integrated luminosity analyzed. This is fully consistent with the one-loop finite mass generated from a 5 TeV Dirac gluino (with $\tilde{r}_3 \simeq 1.5$), as we showed in detail in Sec. III. Importantly, these bounds are only modestly improved with the increased luminosity of the LHC. We emphasize that our luminosity extrapolation was done assuming the search strategies were *unchanged*, and applied to more luminosity at $\sqrt{s} = 7$ TeV. Nevertheless, the clear conclusion from the extrapolation is that the SSSM with a kinematically inaccessible Dirac gluino production remains safe from LHC bounds now and into the near future.

One of the more striking results is that the CMS α_T analysis provided the strongest bound on the squark masses of the SSSM at 1 fb^{-1}. The ATLAS jets plus missing energy search strategy, despite the considerable integrated luminosity 4.7 fb^{-1}, resulted in only a slightly better bound. Our interpretation of these results is that the α_T search, which was designed to maximize signal over background with two jets plus missing energy, provides an ideal search strategy for the SSSM. This is due, in large part, to the fact that the α_T strategy implements a wide range of search channels at intermediate values of H_T that are precisely within the range expected for ~600–800 GeV squarks of the SSSM. This is also borne out by the best bound from the CMS MHT strategy being the lower missing energy, lower H_T channel (distinctly different from the simplified models of the MSSM with lighter gluinos). Examining the expected limits from Fig. 4, we see that the 1 fb^{-1} CMS α_T strategy is expected to yield the same bound on squarks in the SSSM as about a 4 fb^{-1} jets plus missing energy ATLAS analysis. This appears to be because the two jet search strategies done by ATLAS require very large m_{eff}. Indeed, the

ATLAS channel with the best bound on the SSSM (SRA′) has the *least restrictive* cut on m_{eff} (greater than 1200 GeV). Similarly, the CMS *razor* analysis appears to be best optimized for very high mass superpartner searches.

Our study focused on a nearly massless LSP, so that we could perform an apples-for-apples comparison between the LHC bounds on simplified models of the MSSM versus the SSSM. It is interesting to consider how the bounds change as the LSP mass is increased. Since the strongest expected bound on the squark masses in the SSSM comes from the CMS α_T analysis, we explored a variation of the SSSM where we allowed the LSP mass within the range $0 \leq m_{\text{LSP}} \leq 300$ GeV. We find CMS α_T limits for $m_{\text{LSP}} = 100$ GeV are roughly equal to those of a massless LSP. Raising the LSP mass to $m_{\text{LSP}} = 200$ GeV, the squark mass limit drops from 680 GeV to 651 GeV, and we find there is *no* limit for $m_{\text{LSP}} = 300$ GeV. This is consistent with the T2 simplified model studied by CMS [69].

There are many other search strategies for supersymmetry that may be sensitive to more specific models of supersymmetry that have Dirac gaugino masses. Among the often-touted searches for supersymmetry are same-sign dilepton searches, since in the MSSM it is straightforward to obtain a significant same-sign dilepton signature resulting from the chirality flip of a gaugino due to its Majorana mass. In scenarios with Dirac gaugino masses, this source of same-sign dileptons is completely absent. Depending on the implementation of the Higgsino sector, models with Dirac gaugino masses may or may not have effectively small Majorana masses and therefore a suppressed same-sign dilepton signal. It would certainly be interesting to follow up on the SSSM with another simplified model of the electroweak gaugino sector and determine the relative weakness of the LHC bounds. We leave this to future work.

ACKNOWLEDGMENTS

We thank Ricky Fok, Patrick Fox, and Joe Lykken for many valuable conversations. G. D. K. was supported in part by a Ben Lee Fellowship from Fermilab and in part by the U.S. Department of Energy under Contract No. DE-FG02-96ER40969. A. M. and G. K. were supported by Fermilab operated by Fermi Research Alliance, LLC under Contract No. DE-AC02-07CH11359 with the U.S. Department of Energy.

APPENDIX A: SUPERSOFT SUPERSYMMETRIC SIMPLIFIED MODEL

The supersoft supersymmetric simplified model Lagrangian we are considering can be expressed as

$$\mathcal{L} = \mathcal{L}_{\text{kin}} + \mathcal{L}_{\text{yuk}} + \mathcal{L}_{\text{decay}}, \tag{A1}$$

where $\mathcal{L}_{\text{kin}}$ contains the usual squark and gluino kinetic terms, gauge interactions, and masses; $\mathcal{L}_{\text{yuk}}$ contains the gluino-squark-quark interactions; and $\mathcal{L}_{\text{decay}}$ contains the squark-quark-gravitino interactions through which the squarks decay. The kinetic term for the squarks is unchanged from the MSSM, while the gluino is slightly modified to account for the Dirac character of its mass:

$$\mathcal{L}_{\text{kin}} \supset i\bar{\lambda}^a \gamma^\mu (\partial_\mu \delta_{ac} + g_s f^{abc} G^b_\mu)\lambda_c - M_3 \bar{\lambda}^a \lambda_a, \tag{A2}$$

where λ_a is a four-component Dirac bi-spinor. Schematically

$$\lambda_a = \begin{pmatrix} \phi_a \\ \tilde{g}^*_a \end{pmatrix}, \tag{A3}$$

where $\tilde{g}_a$ is the usual gluino, in the sense that it is the superpartner of the gluon, and ϕ_a is the fermionic component of a color-adjoint superfield introduced to get a mass with $\tilde{g}_a$.

The Yukawa terms are the same as in the MSSM; however, if we want to write them in terms of four-component spinors, we need to be careful since matter (squarks and quarks) couples only to $\tilde{g}_a$ and not to ϕ_a:

$$\begin{aligned}\mathcal{L}_{\text{yuk}} = &-\sqrt{2} g_s (\tilde{u}^*_{L,i} t^a \bar{\lambda}_a P_L u_i + \tilde{d}^*_{L,i} t^a \bar{\lambda}_a P_L d_i \\ &- \tilde{u}^*_{R,i} t^a \bar{\lambda}^c{}_a P_R u_i - \tilde{d}^*_{R,i} t^a \bar{\lambda}^c{}_a P_R d_i) + \text{H.c.},\end{aligned} \tag{A4}$$

where t^a are the $SU(3)$ generators, $P_{L,R}$ are the usual chiral projection matrices, and i labels the flavor index.

The gravitino interactions in the SSSM are exactly the same as in the MSSM. Approximating interactions with the gravitino by interactions with its goldstino longitudinal component, we have

$$\mathcal{L}_{\text{decay}} = \frac{i}{\sqrt{3} M_P m_{3/2}} \bar{q}_{\omega,i} \gamma^\mu P_\omega \gamma^\nu D_\nu \tilde{q}_{\omega,i} (\partial_\mu \tilde{G}) + \text{H.c.} \tag{A5}$$

for quark q with helicity ω and flavor i.

In practice, the SSSM contains only two free parameters, the mass of the (Dirac) gluino and the common mass for the first and second generation squarks (both left- and right-handed). The gravitino interaction parameters are irrelevant as we assume the branching fraction of squark to quark plus gravitino to be 100% and the decay is prompt. The Lorentz form of the interactions is important, as it determines the kinematics of the final jets, which in turn sets the acceptance for a given analysis.

APPENDIX B: ACCEPTANCES FOR THE ANALYSES

In this appendix we collect the series of figures showing the acceptances for the various analyses discussed in

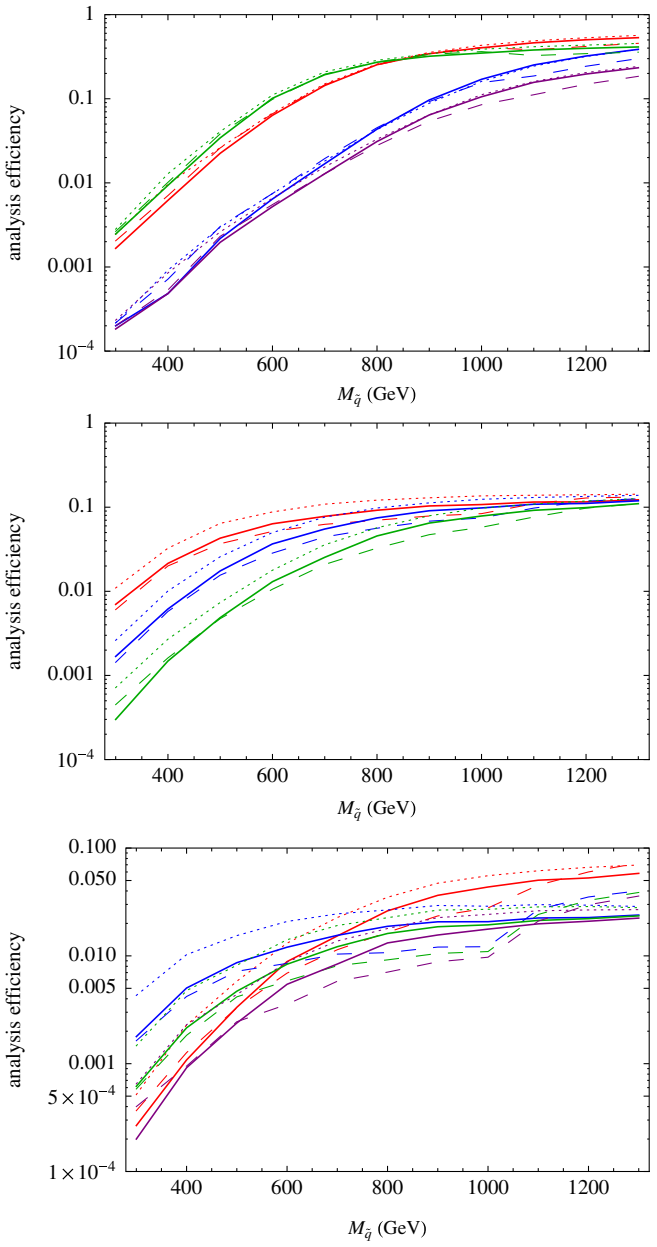

FIG. 5 (color online). Acceptance times efficiency for the 11 channels of the ATLAS analysis. The top panel shows $A \cdot \epsilon$ for the lower multiplicity channels: 2j (A) medium in red (third and fourth lines from the top on the left), 2j (A) tight in blue (fifth and sixth lines from the top on the left), 2j (A′) medium in green (top two lines on the left), and 3j (B) tight in purple. The middle multiplicity (4j) channels are shown in the middle panel: loose m_{eff}(inc) in red (top three lines on the left), medium in blue (middle three lines on the left), tight in green (bottom three lines on the left). Finally, the highest multiplicity channels are shown in the bottom panel: 5j (D) tight in red (top three lines on the right), 6j (E) loose in blue (top three lines on the left), 6j (E) medium in green (middle three lines), and 6j (E) tight in purple (bottom three lines). In all panels, the solid lines correspond to the acceptance times efficiency within the SSSM, the dotted lines correspond to the equal MSSM simplified model with $\tilde{M}_3 = M_{\tilde{q}}$, and the dashed lines correspond to the heavy MSSM simplified model with $\tilde{M}_3 = 5$ TeV.

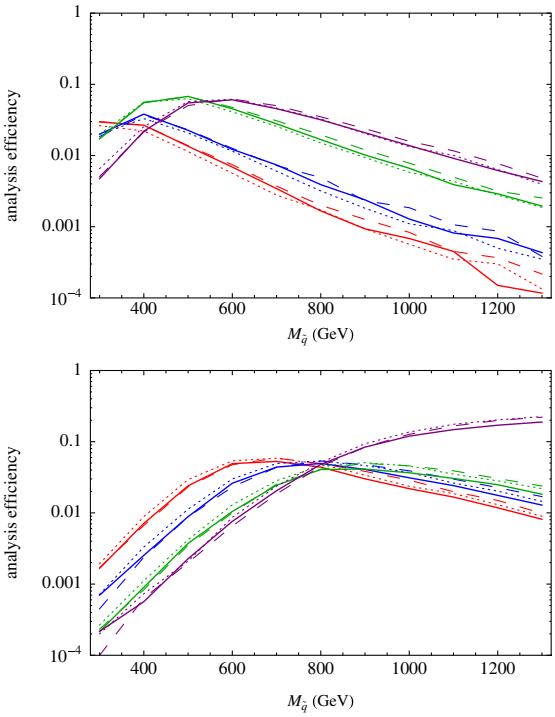

FIG. 6 (color online). Acceptance times efficiency for the SSSM (solid lines), equal MSSM simplified model ($\tilde{M}_3 = M_{\tilde{q}}$) (dotted lines), and heavy MSSM simplified model ($\tilde{M}_3 =$ 5 TeV) (dashed lines) using the CMS α_T analysis. The colors indicate which H_T bin was used. In the top panel, red (lower) lines show $H_T = 275$–325 GeV, blue (next to bottom) lines show 325–375 GeV, green (next to top) lines are for 375–475 GeV, and purple (top) lines are for 475–575 GeV. Similarly, in the bottom panel red (top left to lower right) lines show 575–675 GeV, blue (next to top on left) lines are 675–775 GeV, green (next to bottom on left) lines are 775–875 GeV, and purple (bottom left to top right) are >875 GeV.

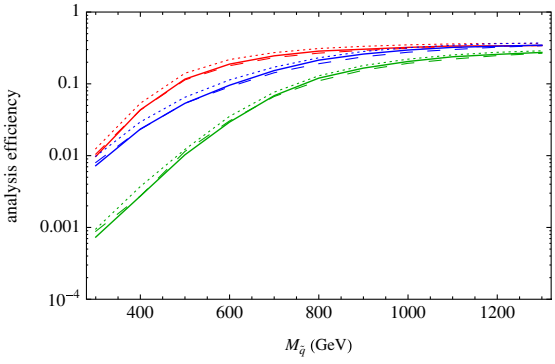

FIG. 7 (color online). Acceptance × efficiency factors for the CMS search based on H_T, $\not{E}_T$. The line hatching follows the same convention as Fig. 6. Red (upper) lines show the limits from baseline selection plus $\not{E}_T > 350$ GeV, $H_T > 500$ GeV; blue (middle) lines show baseline plus $H_T > 800$ GeV; and green (lower) lines show baseline + $\not{E}_T > 500$ GeV, $H_T >$ 800 GeV.

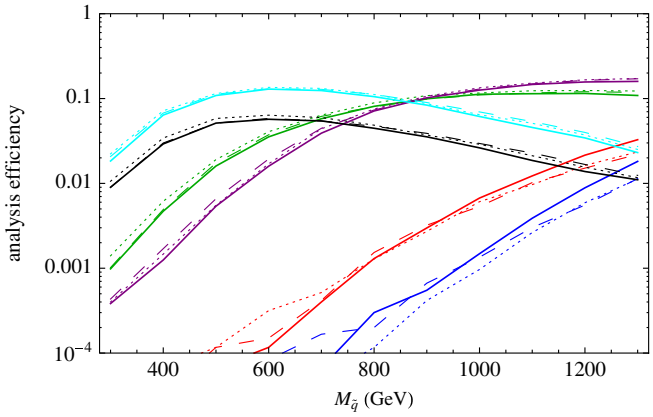

FIG. 8 (color online). Acceptance times efficiency for the CMS search based on the hadronic channel of the *razor* analysis. The line hatching follows the same convention as Fig. 6. The six groups of lines correspond to analyses regions S1 (red, next to bottom), S2 (blue, bottom), S3 (green, third from top on left), S4 (purple, fourth from top on left), S4 (black, second from top on left), and S6 (cyan, top left).

detail in Sec. IV. Figure 5 shows the acceptance for the ATLAS jets plus missing energy search described in Sec. IV A; Fig. 6 shows the acceptance for the CMS α_T search described in Sec. IV B 1; Fig. 7 shows the acceptance for the CMS jets plus missing energy search described in Sec. IV B 2; and Fig. 8 shows the acceptance for the CMS *razor* search described in Sec. IV B 3.

[1] S. Dimopoulos and G. F. Giudice, Phys. Lett. B **357**, 573 (1995).
[2] A. G. Cohen, D. B. Kaplan, and A. E. Nelson, Phys. Lett. B **388**, 588 (1996).
[3] N. Arkani-Hamed, S. Dimopoulos, G. F. Giudice, and A. Romanino, Nucl. Phys. **B709**, 3 (2005).
[4] R. Essig, E. Izaguirre, J. Kaplan, and J. G. Wacker, J. High Energy Phys. 01 (2012) 074.
[5] Y. Kats, P. Meade, M. Reece, and D. Shih, J. High Energy Phys. 02 (2012) 115.
[6] C. Brust, A. Katz, S. Lawrence, and R. Sundrum, J. High Energy Phys. 03 (2012) 103.
[7] M. Papucci, J. T. Ruderman, and A. Weiler, arXiv:1110.6926.
[8] J. L. Feng, K. T. Matchev, and D. Sanford, Phys. Rev. D **85**, 075007 (2012).
[9] C. Csaki, L. Randall, and J. Terning, arXiv:1201.1293.
[10] G. Larsen, Y. Nomura, and H. L. L. Roberts, arXiv:1202.6339.
[11] N. Craig, M. McCullough, and J. Thaler, arXiv:1203.1622.
[12] R. Barbier, C. Bérat, M. Besançon, M. Chemtob, A. Deandrea, E. Dudas, P. Fayet, S. Lavignac, G. Moreau, E. Perez, and Y. Sirois, Phys. Rep. **420**, 1 (2005).
[13] L. M. Carpenter, D. E. Kaplan, and E.-J. Rhee, Phys. Rev. Lett. **99**, 211801 (2007).
[14] C. Csaki, Y. Grossman, and B. Heidenreich, Phys. Rev. D **85**, 095009 (2012).
[15] H. K. Dreiner and T. Stefaniak, arXiv:1201.5014.
[16] B. C. Allanach and B. Gripaios, arXiv:1202.6616.
[17] T. J. LeCompte and S. P. Martin, Phys. Rev. D **84**, 015004 (2011); Phys. Rev. D **85**, 035023 (2012).
[18] J. Fan, M. Reece, and J. T. Ruderman, J. High Energy Phys. 11 (2011) 012; arXiv:1201.4875.
[19] P. Fayet, Phys. Lett. **78B**, 417 (1978).
[20] J. Polchinski and L. Susskind, Phys. Rev. D **26**, 3661 (1982).
[21] L. J. Hall and L. Randall, Nucl. Phys. **B352**, 289 (1991).
[22] P. J. Fox, A. E. Nelson, and N. Weiner, J. High Energy Phys. 08 (2002) 035.
[23] J. Alwall, P. Schuster, and N. Toro, Phys. Rev. D **79**, 075020 (2009).
[24] D. Alves, N. Arkani-Hamed, S. Arora, Y. Bai, M. Baumgart, J. Berger, M. Buckley, B. Butler *et al.*, arXiv:1105.2838.
[25] A. E. Nelson, N. Rius, V. Sanz, and M. Unsal, J. High Energy Phys. 08 (2002) 039.
[26] Z. Chacko, P. J. Fox, and H. Murayama, Nucl. Phys. **B706**, 53 (2005).
[27] L. M. Carpenter, P. J. Fox, and D. E. Kaplan, arXiv:hep-ph/0503093.
[28] I. Antoniadis, A. Delgado, K. Benakli, M. Quiros, and M. Tuckmantel, Phys. Lett. B **634**, 302 (2006).
[29] Y. Nomura, D. Poland, and B. Tweedie, Nucl. Phys. **B745**, 29 (2006).
[30] I. Antoniadis, K. Benakli, A. Delgado, and M. Quiros, Adv. Stud. Theor. Phys. **2**, 645 (2008).
[31] G. D. Kribs, E. Poppitz, and N. Weiner, Phys. Rev. D **78**, 055010 (2008).

[32] S. D. L. Amigo, A. E. Blechman, P. J. Fox, and E. Poppitz, J. High Energy Phys. 01 (2009) 018.
[33] K. Benakli and M. D. Goodsell, Nucl. Phys. **B816**, 185 (2009).
[34] A. E. Blechman, Mod. Phys. Lett. A **24**, 633 (2009).
[35] L. M. Carpenter, arXiv:1007.0017.
[36] G. D. Kribs, T. Okui, and T. S. Roy, Phys. Rev. D **82**, 115010 (2010).
[37] S. Abel and M. Goodsell, J. High Energy Phys. 06 (2011) 064.
[38] C. Frugiuele and T. Gregoire, Phys. Rev. D **85**, 015016 (2012).
[39] H. Itoyama and N. Maru, arXiv:1109.2276.
[40] J. Hisano, M. Nagai, T. Naganawa, and M. Senami, Phys. Lett. B **644**, 256 (2007).
[41] K. Hsieh, Phys. Rev. D **77**, 015004 (2008).
[42] A. E. Blechman and S.-P. Ng, J. High Energy Phys. 06 (2008) 043.
[43] G. D. Kribs, A. Martin, and T. S. Roy, J. High Energy Phys. 01 (2009) 023.
[44] S. Y. Choi, M. Drees, A. Freitas, and P. M. Zerwas, Phys. Rev. D **78**, 095007 (2008).
[45] T. Plehn and T. M. P. Tait, J. Phys. G **36**, 075001 (2009).
[46] R. Harnik and G. D. Kribs, Phys. Rev. D **79**, 095007 (2009).
[47] S. Y. Choi, M. Drees, J. Kalinowski, J. M. Kim, E. Popenda, and P. M. Zerwas, Phys. Lett. B **672**, 246 (2009).
[48] G. D. Kribs, A. Martin, and T. S. Roy, J. High Energy Phys. 06 (2009) 042.
[49] G. Belanger, K. Benakli, M. Goodsell, C. Moura, and A. Pukhov, J. Cosmol. Astropart. Phys. 08 (2009) 027.
[50] K. Benakli and M. D. Goodsell, Nucl. Phys. **B830**, 315 (2010).
[51] A. Kumar, D. Tucker-Smith, and N. Weiner, J. High Energy Phys. 09 (2010) 111.
[52] E. J. Chun, J.-C. Park, and S. Scopel, J. Cosmol. Astropart. Phys. 02 (2010) 015.
[53] K. Benakli and M. D. Goodsell, Nucl. Phys. **B840**, 1 (2010).
[54] R. Fok and G. D. Kribs, Phys. Rev. D **82**, 035010 (2010).
[55] A. De Simone, V. Sanz, and H. P. Sato, Phys. Rev. Lett. **105**, 121802 (2010).
[56] S. Y. Choi, D. Choudhury, A. Freitas, J. Kalinowski, J. M. Kim, and P. M. Zerwas, J. High Energy Phys. 08 (2010) 025.
[57] S. Y. Choi, D. Choudhury, A. Freitas, J. Kalinowski, and P. M. Zerwas, Phys. Lett. B **697**, 215 (2011); **698**, 457(E) (2011).
[58] R. Davies, J. March-Russell, and M. McCullough, J. High Energy Phys. 04 (2011) 108.
[59] K. Benakli, M. D. Goodsell, and A.-K. Maier, Nucl. Phys. **B851**, 445 (2011).
[60] P. Kumar and E. Ponton, J. High Energy Phys. 11 (2011) 037.
[61] M. Heikinheimo, M. Kellerstein, and V. Sanz, J. High Energy Phys. 04 (2012) 043.
[62] B. Fuks, Int. J. Mod. Phys. A **27**, 1230007-1 (2012).
[63] G. Aad *et al.* (ATLAS Collaboration), Phys. Lett. B **710**, 67 (2012); Report No. ATLAS-CONF-2012-033.
[64] S. Chatrchyan *et al.* (CMS Collaboration), Phys. Rev. Lett. **107**, 221804 (2011).
[65] CMS Collaboration, Report No. CMS-PAS-SUS-11-004.
[66] S. Chatrchyan *et al.* (CMS Collaboration), Phys. Rev. D **85**, 012004 (2012); Report No. CMS-PAS-SUS-12-005.
[67] T. Sjostrand, S. Mrenna, and P. Z. Skands, J. High Energy Phys. 05 (2006) 026.
[68] S. Ovyn, X. Rouby, and V. Lemaitre, arXiv:0903.2225.
[69] https://twiki.cern.ch/twiki/bin/view/CMSPublic/PhysicsResultsSUS11003.
[70] W. Beenakker, R. Hopker, M. Spira, and P. M. Zerwas, Nucl. Phys. **B492**, 51 (1997); W. Beenakker, M. Kramer, T. Plehn, M. Spira, and P. M. Zerwas, Nucl. Phys. **B515**, 3 (1998); W. Beenakker, M. Klasen, M. Kramer, T. Plehn, M. Spira, and P. M. Zerwas, Phys. Rev. Lett. **83**, 3780 (1999); **100**, 029901(E) (2008); M. Spira, arXiv:hep-ph/0211145; T. Plehn, Czech. J. Phys. **55**, B213 (2005).
[71] J. Conway and K. Maeshima, Report No. CDF/PUB/EXOTIC/PUBLIC/4476.
[72] J. Conway, Report No. CDF/PUB/STATISTICS/PUBLIC/6428.
[73] K. Cranmer and I. Yavin, J. High Energy Phys. 04 (2011) 038.
[74] G. Aad *et al.* (Atlas Collaboration), J. High Energy Phys. 11 (2011) 099; Report No. ATLAS-CONF-2012-037.
[75] C. Rogan, arXiv:1006.2727.